Journal of Membrane Science 385–386 (2011) 234–242

Contents lists available at SciVerse ScienceDirect

Journal of Membrane Science

journal homepage: www.elsevier.com/locate/memsci

Power generation using profiled membranes in reverse electrodialysis

David A. Vermaas[a,b], Michel Saakes[a], Kitty Nijmeijer[b,*]

[a] Wetsus, Centre of Excellence for Sustainable Water Technology, P.O. Box 1113, 8900 CC Leeuwarden, The Netherlands
[b] Membrane Science & Technology, University of Twente, P.O. Box 217, 7500 AE Enschede, The Netherlands

ARTICLE INFO

Article history:
Received 1 July 2011
Received in revised form
26 September 2011
Accepted 29 September 2011
Available online 5 October 2011

Keywords:
Ion exchange membranes
Profiled membranes
Reverse electrodialysis
Salinity gradient energy
Spacers

ABSTRACT

Reverse electrodialysis (RED) is a technology to obtain energy from the salinity difference between salt water and fresh water. Traditionally, ion exchange membranes, separated by non-conductive spacers, are used in this technology. As an alternative for these non-conductive spacers, in this work, heterogeneous ion exchange membranes were hot pressed in the dry state to create a profiled membrane comprising 230–245 μm ridges (in wet state) on one side of the membrane. Stacking such profiled membranes creates channels for the feed water, thus make the use of spacers obsolete. The performance of a RED-stack with such profiled membranes was compared for the first time with a RED-stack with traditional, non-conductive spacers. The ohmic resistance was significantly lower for the stack with profiled membranes compared to that with spacers, whereas the boundary layer resistance was higher. This resulted in slightly higher power densities for the stack with profiled membranes. Despite this small improvement, profiled membranes have a strong future development potential. Experimental data show that the hydraulic friction is much lower for the stack with profiled membranes and hence higher Reynolds numbers are possible than in a stack with spacers. Furthermore, profiling membranes allow much freedom to create new profile geometries where a hydrodynamic flow can be combined with efficient mixing in the boundary layers.

1. Introduction

Reverse electrodialysis (RED) is a renewable energy source that uses the energy from the mixing of salt and fresh water. This Gibbs free energy of mixing is available when concentrated and diluted salt solutions mix and RED captures this salinity gradient energy using ion exchange membranes.

The principle of RED has been described by several authors [1–3]. A RED stack is comprised of an alternating series of cation exchange membranes (CEMs) and anion exchange membranes (AEMs). When alternating concentrated and diluted salt solution flow in between the ion exchange membranes, ions are transported from the concentrated to the diluted compartment, forced by the salinity gradient. Since the ion exchange membranes ideally only allow either positive or negative ions to pass, cations are transported to one side and anions to the other side. The resulting potential difference over the membranes can be used to power an electrical device.

To make RED an economically attractive technology to extract energy from the mixing of sea and river water, the net power to be generated per membrane area (i.e. net power density) is estimated to be 2 W/m^2 at a fuel efficiency of 70% [4]. Previous research already showed that 80% fuel efficiency is possible [2]. The net power density in RED was recently increased to 1.2 W/m^2 [5]. Although this was almost twice the highest value reported previously, it is still considerably lower than the aimed 2 W/m^2. A high power density will reduce the price since the membrane costs are dominant compared to the other costs in a large scale RED power plant [4]. The fuel efficiency is of minor importance for a first plant, as water flows are not limiting yet.

To achieve a high net power density, the internal resistance of the system and the hydraulic friction of the feed waters in the compartments should be low. A low internal resistance minimizes the electrical loss in the stack and a low hydraulic friction of the feed waters minimizes the pumping power. The non-conducting spacers, which are traditionally used to keep the membranes separated, significantly increase the internal resistance and the hydraulic friction of the feed waters.

A non-conductive spacer made from materials such as PET (polyethylene terephthalate), covers a part of the membrane and reduces the membrane area available for ion conduction. This is known as the spacer shadow effect [6]. Furthermore, the ionic current through the spacer grid is tortuous, which lengthens the current streamlines and thus increases the electrical resistance. Due to the presence of non-conductive spacers, the internal resistance in previous experiments was more than twice the value

* Corresponding author. Tel.: +31 53 489 4185.
E-mail address: d.c.nijmeijer@utwente.nl (K. Nijmeijer).

0376-7388/$ – see front matter © 2011 Elsevier B.V. All rights reserved.
doi:10.1016/j.memsci.2011.09.043

expected based on the conductivity of the individual components [6,7].

In addition, the knits of the spacers (where the spacer filaments cross) are a major source of hydraulic friction of the feed waters; experimental values exceed the theoretical equivalents for uniform laminar flow by more than an order of magnitude [5,8]. Consequently, the power spent on pumping of the feed waters is significant compared to the actual power generated. In addition, spacers are vulnerable to biofouling, which increases the hydraulic friction even more. Biofouling is recognized as a spacer problem rather than a membrane problem [9,10].

Ion-conductive spacers reduce the internal resistance (e.g. [6,11]), but do not reduce the hydraulic friction. Profiled membranes on the other hand, i.e. membranes with a relief on their surface integrating the spacer and membrane functionality, make the use of separate spacers obsolete since the profile keeps the membranes separated while providing channels for the feed waters. Such profiled membranes (sometimes referred to as corrugated membranes) can combine a low internal resistance due to their ion-conducting ridges with a low hydraulic friction.

Profiled membranes have been used incidentally in electrodialysis (ED) [12–14]. The internal resistance in these experiments was approximately 1.6 times lower for a stack with double sided profiled membranes when compared to a system with non-conductive spacers [14]. At higher feed water concentrations, the difference with non-conductive spacers became less pronounced. Higher limiting currents were found for devices with profiled membranes [14] due to the increase in available area for ion exchange. Profiled membranes show also a lower hydraulic friction in ED when compared to a device with spacers [13].

So far, profiled membranes have not been used in reverse electrodialysis and the results found in ED cannot be adopted a priori in RED, because the inter-membrane distance and the Reynolds numbers in RED are significantly smaller than in ED; Reynolds numbers in RED are usually an order of magnitude smaller than those in ED. Moreover, phenomena like the overlimiting current and water splitting are absent in RED.

Here we investigate for the first time the operation of a RED stack with profiled membranes, and compare its performance to that of a RED stack with non-conductive spacers. The open circuit voltage, internal resistance and hydraulic friction of the feed waters are experimentally determined for both stacks, which enables comparing both stacks in terms of (net) power density and fuel efficiency.

2. Theory

The gross power density that can be obtained from a RED stack is related to the electromotive force E (V) that follows from the concentration difference over the membrane, the current density J (A/m^2) and the ohmic area resistance R_{ohmic} (Ω m^2), according to:

$$P_{gross} = \frac{E \cdot J - R_{ohmic} \cdot J^2}{N_m} \quad (1)$$

In which P_{gross} is the gross power density (in W/m^2 membrane) and N_m is the number of membranes. The electromotive force is given by the Nernst equation (as a theoretical voltage over the membranes due to different ion activities at either side of a membrane) and corrected for the membrane permselectivity and the number of membranes [15].

When no current is applied, the electromotive force can be estimated based on the inflow concentrations of the feed waters. This yields the open circuit voltage (E_{OCV}). When a current is applied, ions exchange from the salt water to the fresh water, and the concentrations at the membrane surface will be different than the concentration at the feed water inflow. Due to the process of ion exchange, the concentrations of the feed water compartments will approach each other. Hence, the electromotive force will be lower than the E_{OCV}. We can subdivide this potential reduction into a part due to the concentration change in the (concentration) boundary layer, E_{BL}, and a part due to the concentration change in the bulk solution, $E_{\Delta C}$. The equation for the gross power density can thus be written as:

$$P_{gross} = \frac{(E_{OCV} - E_{BL} - E_{\Delta C}) \cdot J - R_{ohmic} \cdot J^2}{N_m} \quad (2)$$

In which E_{OCV}, E_{BL} and $E_{\Delta C}$ are in Volt. The impact of E_{BL} and $E_{\Delta C}$ can be compared to the ohmic resistance if E_{BL} and $E_{\Delta C}$ are divided by the current density. The reduction in electromotive force, divided by the current density, is than interpreted as a (non-ohmic) resistance:

$$P_{gross} = \frac{E_{OCV} \cdot J - R_i \cdot J^2}{N_m} \quad (3)$$

with

$$R_i = R_{ohmic} + R_{\Delta C} + R_{BL} \quad (4)$$

In which R_i is the total internal area resistance (Ω m^2), $R_{\Delta C}$ is the contribution to the resistance due to the concentration change in the bulk solution (Ω m^2) and R_{BL} is the boundary layer resistance (Ω m^2). The boundary layer resistance, R_{BL}, is associated with concentration polarization [6,16]. The contribution of $R_{\Delta C}$ was often not recognized in previous research (e.g. [2,6]), but is significant in RED [5].

The values of R_i and R_{ohmic} can be determined experimentally from chrono-potentiometric experiments [5,16]. The total internal resistance, R_i, is derived from the (stationary) voltage when a stable current is applied. The sudden jump in voltage when the current is released reveals the contribution of the ohmic resistance. The latter time dependent voltage change is due to R_{BL} and $R_{\Delta C}$.

The contribution of $R_{\Delta C}$ can be estimated from [5]:

$$R_{\Delta C} = \frac{N_m}{2} \cdot \frac{\alpha \cdot R \cdot T}{F \cdot J} \cdot \ln\left(\frac{\Delta a_r}{\Delta a_s}\right) \quad (5)$$

In which $\Delta a_r = 1 + ((J \cdot A)/(F \cdot \Phi_r \cdot c_r))$ and $\Delta a_s = 1 - ((J \cdot A)/(F \cdot \Phi_s \cdot c_s))$, α is the apparent permselectivity (as defined in e.g. [15]) R is the universal gas constant (8.314 J/mol/K), T is the absolute temperature (K), F is the Faraday constant (96,485 C/mol), A is the electrode area (m^2), Φ is the discharge of the feed water per compartment (m^3/s), c is the inflow concentration of the feed waters (mol/m^3) and the subscripts r and s refer to river water and seawater, respectively. The last contribution, the boundary layer resistance (R_{BL}), can subsequently be derived as the remaining contribution in Eq. (4).

Next to the power generated by the RED stack, power is consumed to pump the feed water through the stack. The pumping power per membrane area, P_{pump} (W/m^2 membrane), can be calculated as [17]:

$$P_{pump} = \frac{\Delta p_r \cdot \Phi_r + \Delta p_s \cdot \Phi_s}{2A} \quad (6)$$

In which Δp is the pressure drop in the feed water over the RED stack (Pa). The factor $2A$ originates from the membrane area of cation and anion exchange membranes together. The pressure drop for a fully developed, uniform and laminar flow in an infinite wide channel can be calculated by using a momentum balance containing the pressure gradient and the wall friction. This theoretical pressure drop is given by [5]:

$$\Delta p = \frac{12\mu \cdot L \cdot \Phi}{b \cdot d^3} \quad (7)$$

In which μ is the viscosity of water (Pa s), L is the length of the flow path (m), b is the width of the flow path (m) and d is the height of the flow path (m). Under experimental conditions and

especially in spacer filled channels, the pressure drop can be significantly higher than this theoretical value [5]. Consequently, this theoretical value is considered as a minimum value, corresponding to optimum (uniform, infinite wide) circumstances.

The net power density is the difference between the maximum value from Eq. (3) (gross power density) and Eq. (6) (power losses by pumping):

$$P_{net} = \frac{E_{OCV}^2}{4N_m \cdot R_i} - \frac{\Delta p_r \cdot \Phi_r + \Delta p_s \cdot \Phi_s}{2A} \quad (8)$$

Profiled membranes are expected to lower the ohmic resistance, and thus the total resistance R_i, by providing ion conducting pathways in stead of a spacer shadow when using non-conductive spacers. Furthermore the pressure drop, Δp, is expected to be lower using profiled membranes compared to stacks with flat membranes and spacers, due to the absence of spacer filaments disturbing the flow. Therefore, the net power density is expected to be higher for a stack with profiled membranes when compared to a stack with flat membranes and spacers.

3. Experimental setup

3.1. Membranes

Commercial heterogeneous membranes, types Ralex CMH and AMH (Mega a.s., Czech Republic) were used. These membranes are composed of a polyethene (PE) substrate with ion exchange resins and polyethersulfone (PES) re-inforcement incorporated. Although the resistance of these membranes is relatively high compared to that of homogeneous ion exchange membranes [15], these membranes were selected because of their relatively low melting temperature of approximately 115 °C. This offers the possibility to apply a profile in the membrane in dry form using hot pressing at relatively low temperatures.

The resistance and permselectivity of the membranes were measured before and after hot pressing of the membranes. The membrane resistance was measured in 0.5 M NaCl. The permselectivity was measured using 0.1 M NaCl and 0.5 M NaCl. The experimental setup for membrane resistance and permselectivity determination is described elsewhere [15].

3.2. Membrane profiling

To create the one-sided profiled membranes, the dry membranes were cut in pieces of 160 mm × 160 mm and sandwiched between two aluminum moulds. One of these moulds had a profile comprising of channels of 200 μm in depth and 200 μm in width, as shown in Fig. 1. The other mould had a chamber with a flat bed of 164 mm × 164 mm in size and 220 μm in depth.

A release agent (EWO 7902, KVS, Germany) was sprayed on the membranes to facilitate release of the membranes from the moulds after hot pressing. The moulds and membranes were placed in a thermal press (Vogt Maschinenbau, Germany), which was preheated to 140 °C. The moulds were heated for 2 min, and subsequently pressed for 10 min at 53 tons. The pressure on the total area of 160 mm × 160 mm was 210 bar. Finally, the moulds were cooled to 40 °C and removed from the press.

The use of a thermal press to apply the profile on the membranes could alter the characteristics of the membrane [18]. To exclude this effect, also the membranes used in the stack with spacers were hot pressed according to the same procedure. In this case, the same mould with a 220 μm deep chamber was used on one side, while the other side was covered by a flat aluminum plate.

The pressed membranes were immersed in demineralized water, ultrasonically treated in approximately 0.25 M NH_3 to remove the release agent, rinsed in demineralized water, immersed in 3 M NaCl to exchange the counter ions in the membranes towards Na^+ or Cl^-, and finally immersed in 0.25 M NaCl to equal conditions in the stack. The final, wet membranes have ridges with a height of 245 ± 5 μm for the CEMs and 230 ± 5 μm for the AEMs.

3.3. Stack

A schematic picture of the stack with profiled membranes and that with spacers is given in Fig. 2.

Both stacks contained 2 Ti electrodes (mesh 1.0, 10 cm × 10 cm) coated with Ir/Ru (Magneto Special Anodes B.V., The Netherlands), two CEMs (Neosepta, CMX) shielding the electrode compartments, and two buffer compartments (Fig. 2) to prevent leakage of the electrolyte towards the feed waters and vice versa.

The stack with the profiled membranes contained 5 profiled CEMs and 5 profiled AEMs, alternately stacked. A silicone film of 100 μm (Specialty Silicone Fabricators, USA), that fits around the profiled area, was used to seal the water compartments in the stack with profiled membranes. In case of the stack with spacers, 5 flat (pressed) CEMs and 5 flat (pressed) AEMs were alternately stacked. A woven fabric, non-conductive spacer (Sefar Nitex 07-300/46, Switzerland), was cut in the same shape (Fig. 2) as the profiled area of the profiled membranes. The thickness of this spacer was 240 ± 5 μm as measured using a thickness gage (Mutitoyo 547-401, Japan). According to the specifications of the manufacturer, the open area of the spacer was 46% and its porosity was 72%. A silicone film (Specialty Silicone Fabricators, USA) of approximately 250 μm thick was used to seal the water compartments.

3.4. Feed waters

Synthetic feed water representatives for seawater and river water with a concentration of 0.507 M (i.e. 3.00%) and 0.017 M (i.e. 0.10%) NaCl, respectively, were prepared by dissolving NaCl (technical grade, ESCO, The Netherlands) in demineralized water. The feed solutions were kept at 25 ± 0.5 °C by a heater (Tetratec HT300, Germany) and a pump.

The artificial sea and riverwater solutions were pumped through the stack by two adjustable peristaltic pumps (Cole-Parmer, Masterflex L/S Digital drive, USA). Measurements were performed at 0.8, 1.5, 3, 5, 8, 15, 30, 60, 100, 150, 200 and 250 ml/min. A 1 μm cartridge filter was placed in a two liter container just before the stack, not only for filtering, but rather to dampen the pressure pulse created by the peristaltic pumps.

For each flow rate, the Reynolds number was calculated being defined as the Reynolds number for a wide slit:

$$Re = \frac{\bar{u} \cdot D_h}{\nu} = \frac{\bar{u} \cdot 2d}{\nu} = \frac{2\Phi}{b \cdot \nu} \quad (9)$$

where $\bar{u}$ is the average flow velocity, D_h is the hydraulic diameter and ν is the kinematic viscosity of water (8.9×10^{-7} m^2/s at 25 °C).

The pressure drop between the inflow and outflow of the feed waters was measured using a differential pressure meter (Endress + Hauser Deltabar S, Germany) with an accuracy of 0.1 kPa ± 1%.

3.5. Electrode and buffer compartments

The electrode rinse solution was composed of 0.05 M $K_3Fe(CN)_6$, 0.05 M $K_4Fe(CN)_6$ and 0.5 M NaCl, and circulated at 400 ml/min from one electrode compartment to the other electrode compartment and back to its storage vessel.

The buffer compartments were fed with 0.5 M NaCl circulating at 80 ml/min and kept at 1 bar by a pressure control valve. In this way, the pressure outside of the membranes is always higher than

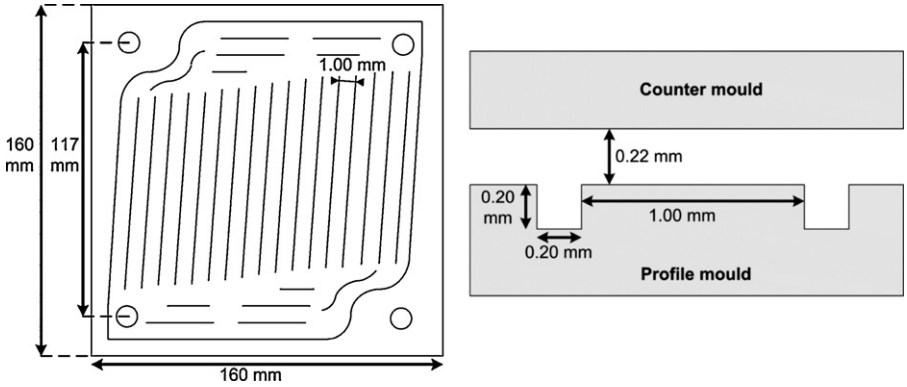

Fig. 1. Drawing of moulds. Left: top view of profile mould (not on scale). The black lines indicate the grooves in the mould. Right: cross section at the middle of the moulds.

that in the interior, ensuring that the membranes remain closely packed.

The electrode rinse solution and buffer solution were kept at $25 \pm 0.2\,^{\circ}C$ using a water bath (Haake DC10, Germany). The complete stack, including the filters for the feed water, was placed in a thermostatic chamber (MMM Friocell 222, Germany) to maintain the temperature at $25.0 \pm 0.1\,^{\circ}C$ during operation.

3.6. Electrical characterization

Chronopotentiometry was performed on both stacks. At least 4 current steps were applied for every flow rate using a galvanostat (Ivium Technologies, The Netherlands). The level and duration of the current steps were different for all flow rates to ensure that equilibrium was reached. At the lowest flow rate, 0.8 ml/min, the current steps ranged from 2.5 to 10 A/m^2 and each level was imposed for 7200 s. At the highest flow rate of 250 ml/min, the current steps ranged from 5 to 30 A/m^2 and lasted 50 s each, which was already sufficient to reach equilibrium at this flow rate.

A part of the internal resistance of the system is due to the resistance of the electrodes and buffer compartments. These resistances are not of interest for a full-scale application, where many more membrane pairs can be stacked and the contribution of the electrodes and corresponding compartments is small compared to that of the other resistances. However, in a lab-scale stack these resistances do play a role and should be taken into account. As such, the total internal area resistance of the system is corrected for the resistance of the electrodes and buffer compartments. The resistance of the electrodes and buffer compartments was measured using an 'empty' stack, consisting of two electrodes, two electrode compartments and two buffer compartments only. Chronopotentiometry was conducted on this empty stack under the same conditions as for the RED stacks.

Fig. 3 shows a typical example of the experimental data obtained for the resistance and the corresponding gross power density, as a function of the current density.

The total area resistance is often assumed to be independent of the current density, which would result in a single parabolic graph for the gross power density when plotted against the current density (Eq. (3)) [19–21]. However, Fig. 3 shows that the resistance is not constant for different current densities, and thus the estimated maximum gross power density is differs, depending on the current density used to measure the resistance. All components of the resistance decrease if the current density increases, with a most significant decrease in R_{BL}. The decrease in resistance is due to ion transport and the corresponding increase in conductivity of the fresh water. The resistance has a stronger dependency on the current density at lower Reynolds numbers or flow rates, whereas

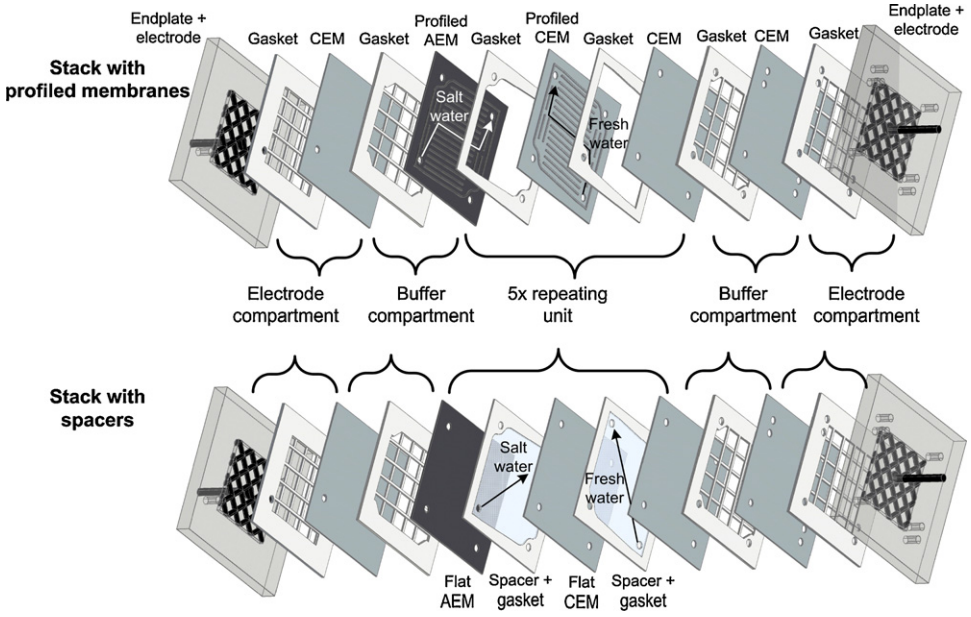

Fig. 2. Illustration of stack setup with profiled membranes (upper part) and that with spacers (bottom part).

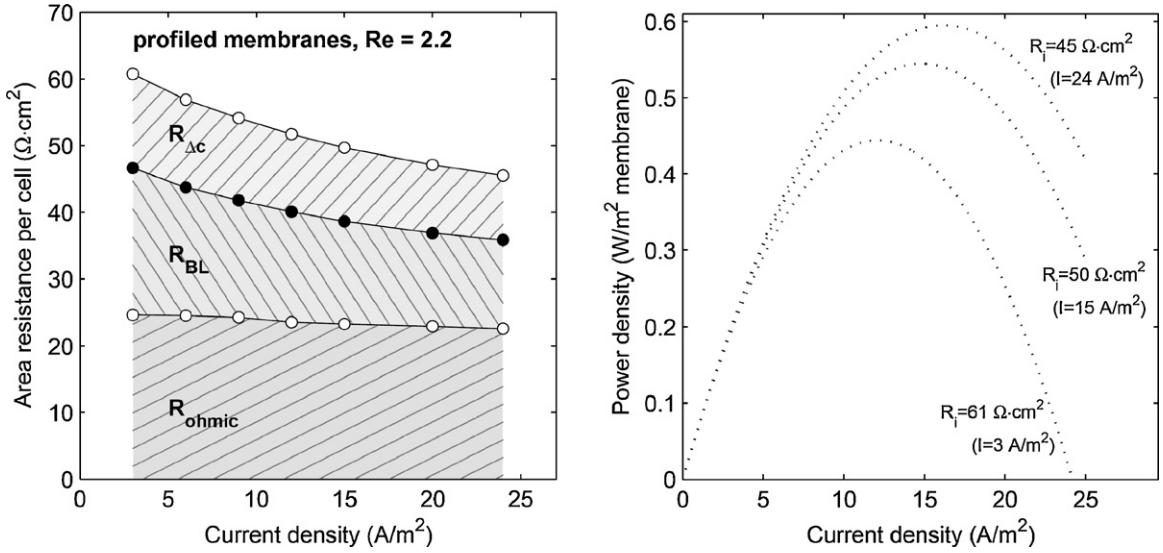

Fig. 3. Typical example of area resistance and gross power density as a function of the current density, for a stack with profiled membranes, at a Reynolds number of 2.2.

the resistance is hardly influenced by the current density at higher flow rates when the feed waters are rapidly renewed. For a typical Reynolds number in RED, as in Fig. 3, the maximum power density can be estimated 10% lower or higher when the resistance is measured at a suboptimal current density. Consequently, the representative resistance is measured at a current density corresponding to the maximum power density.

Using the open circuit voltage and the resistances as determined experimentally, the maximum power density output can be calculated using Eq. (3). Subtracting the pumping power losses, the net power density can be calculated using Eq. (8).

All measurements were performed in duplicate, i.e. on two individual stacks with profiled membranes and two stacks with spacers. The average values are presented, with error bars at one standard deviation to indicate the fluctuations. Some error bars are smaller than the symbol size and therefore not visible.

4. Results and discussion

4.1. Profiled membrane characteristics

Table 1 shows the specifications of the manufacturer and the measured permselectivity and resistance of the membranes, before and after hot pressing. The permselectivity and resistance do change after hot pressing, most drastically in the case of the AEMs (AMH). The differences between the profiled membranes and the corresponding flat pressed membranes are nevertheless small. This emphasizes that a RED-stack with profiled membranes needs to be compared to a RED-stack with flat pressed membranes only.

The changes occurring in the membranes due to hot pressing are not the main focus of this research and will not be discussed in detail. Hot pressing is not the only method available for profiled membrane production and other methods, e.g. casting [22,23], could be used as well. Nevertheless, some explanations for the observations in Table 1 can be suggested. The reduced membrane resistance after hot pressing is mainly caused by the lower thickness of the membranes. For AMHs, the specific conductivity increased after pressing, while the permselectivity decreased. Previous research showed that the membrane surface area covered by ion exchange resin particles was reduced after hot pressing of heterogeneous ion exchange membranes [18]. This suggests a lower surface charge and hence a lower permselectivity. To obey continuity of mass, ion exchange particles will become more closely packed in the cross sectional direction, which may explain a slightly higher specific conductivity.

Fig. 4 shows scanning electron microscope (SEM) images of dry profiled cation and anion exchange membranes.

The ridges of the dry profiled membrane are as expected 200 (±5) μm in height, corresponding to the mould grooves. The width of the ridges is slightly more than 200 μm, especially at the ridge foot. The ridges expand in wet state to a height of 245 ± 5 μm for the CEMs and 230 ± 5 μm for the AEMs.

4.2. Power density

Fig. 5 shows the gross power density of the stacks with profiled membranes and that with spacers as a function of the Reynolds number and the fuel efficiency (i.e. the actual generated energy per liter feed water compared to the theoretical equivalent).

Table 1
Properties of Ralex CMH and AMH.

Membrane	Area resistance (Ω cm²)	Permselectivity (%)	Wet thickness (μm)	Conductivity (mS/cm)
CMH-PES				
Specification	<10	>92	<700	>6.3
Measured, unpressed	7.0 ± 0.3	97 ± 2	650 ± 15	9.3 ± 0.3
Measured, flat pressed	5.8 ± 0.3	95 ± 1	570 ± 25	9.8 ± 0.4
Measured, profiled	5.4 ± 0.3	95 ± 1	510 ± 15[a]	9.3 ± 0.5
AMH-PES				
Specification	<7.5	>90	<750	>8.3
Measured, unpressed	7.3 ± 0.3	89 ± 1	670 ± 15	9.1 ± 0.3
Measured, flat pressed	3.5 ± 0.3	87 ± 1	485 ± 15	13.9 ± 0.6
Measured, profiled	2.7 ± 0.1	87 ± 1	475 ± 10[a]	17.7 ± 0.6

[a] Thickness of membrane excluding ridges. The ridges were 245 ± 5 μm (CEM) and 230 ± 5 μm (AEM) high.

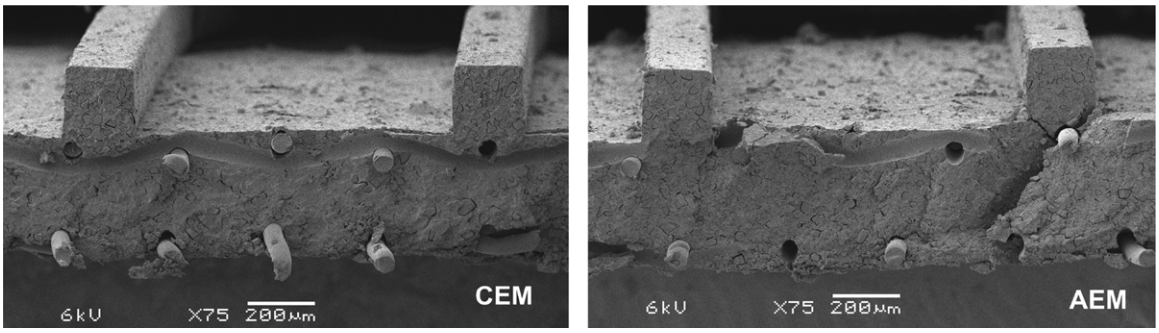

Fig. 4. Representative SEM-image of cross-section of the profiled CEM (CMH) left and AEM (AMH) right. The protruding fibers and black holes are remnants of the reinforcement (PES) in the membrane. The small crack in the AEM is due to cutting of the membrane.

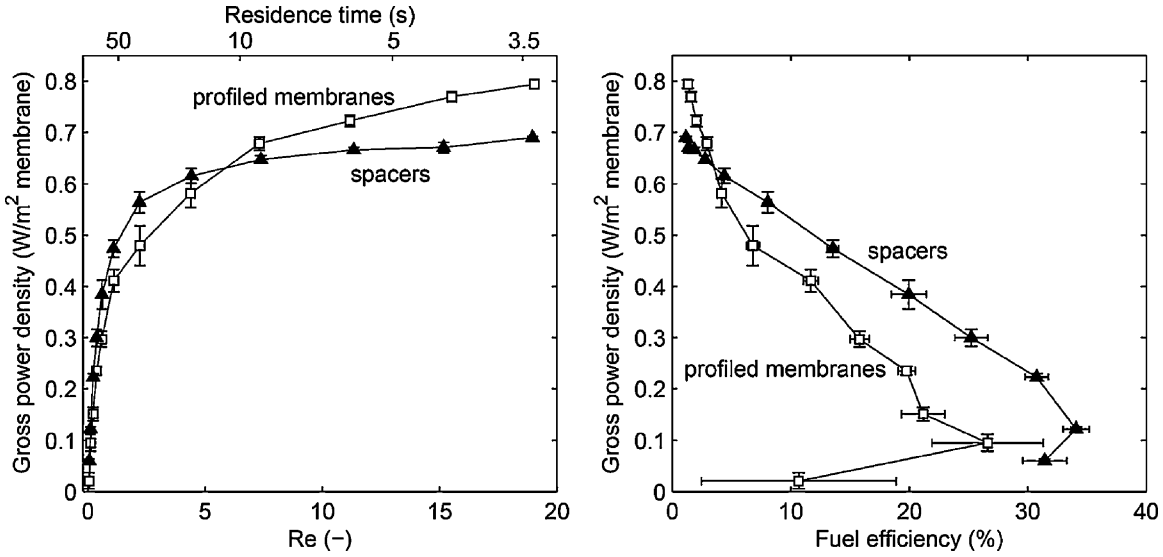

Fig. 5. Power density as a function of the Reynolds number and fuel efficiency, for a stack with profiled membranes and a stack with spacers.

The gross power density increases with increasing Reynolds number since the internal resistance decreases with increasing Reynolds number. At higher Reynolds numbers, the power density of the stack with profiled membranes is higher than that obtained for the stack with spacers, whereas the stack with spacers gives the highest power densities at lower Reynolds numbers. The power density for the stack with spacers only increases slightly for residence times smaller than 10 s, which is in agreement with previous observations [15,17]. The stack with profiled membranes on the other hand shows a much steeper increase in gross power density at lower residence times. This shows that the power density of a RED stack with profiled membranes can exceed the power density for a stack with spacers even more at higher Reynolds numbers (i.e. very high flow rates and lower residence times).

This observation is reflected in the fuel efficiency as well. At high flow rates, the stack with profiled membranes generates higher power densities at the expense of the fuel efficiency compared to the stack with spacers. At high fuel efficiencies (low flow rates), the stack with spacers yields a higher power density. The maximum fuel efficiency was found for the one but lowest flow rate. At the lowest flow rate, losses due to co-ion transport and osmosis reduce the fuel efficiency again, as was demonstrated previously [17].

For a small-scale power plant, where not the amount of water but the price of the plant limit the process, low fuel efficiencies are acceptable to generate high power densities. Profiled membranes give a higher gross power density in that range. When the supply of water becomes limiting, higher fuel efficiencies are desired.

4.3. OCV

To explain the differences in gross power density for the stack with profiled membranes and that with spacers, the OCV and the

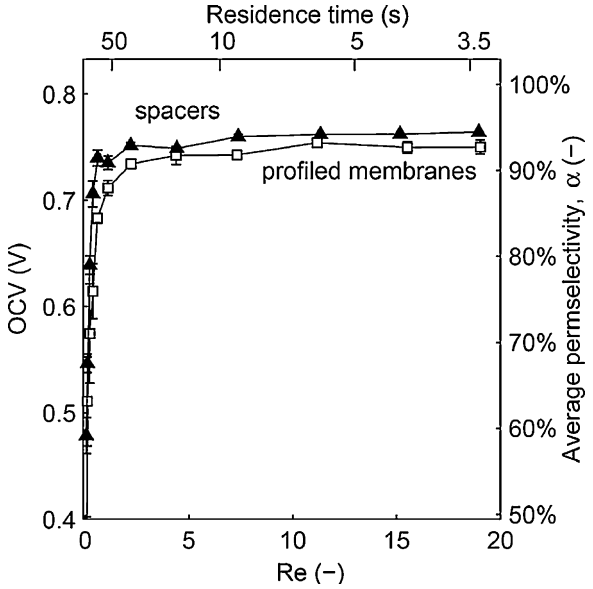

Fig. 6. Open circuit voltage (OCV) as a function of the Reynolds number, for a stack with profiled membranes and one with spacers.

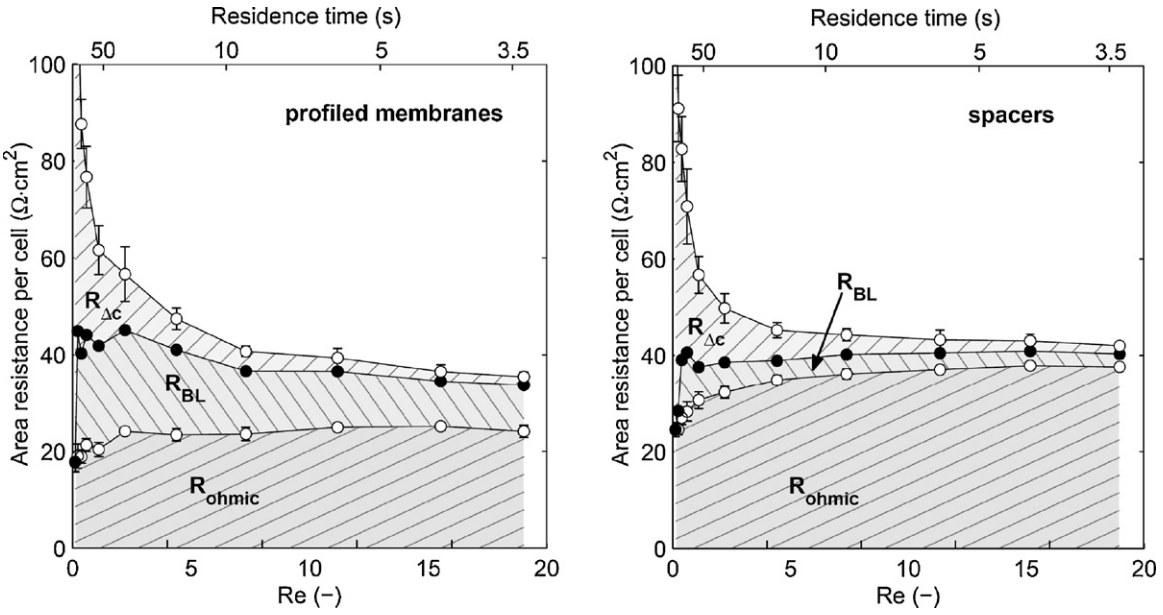

Fig. 7. Area resistance as a function of the Reynolds number, for a stack with profiled membranes and a stack with spacers.

resistance of both stacks are examined. Fig. 6 shows the OCV for the stack with profiled membranes and that with spacers.

At high Reynolds numbers, the values found for the OCV are approximately 92–94% of the theoretical value as derived from the Nernst equation, whereas significantly lower values are measured at low flow velocities. Długołęcki et al. [20] reported similar behavior. They explained the low OCV at low flow velocities by referring to concentration polarization. Although this term is somewhat ambiguous for open circuit conditions (no net charge transport), the OCV is indeed limited by changes in concentration in the vicinity of the membranes, which is most pronounced at low flow velocities. The non-perfect membranes allow small fluxes of water from the river water compartments to the seawater compartments and salt transport (co-ion and counter-ion) from the seawater to the river water compartment are apparent as well. This transport is assumed to be confined in a relatively small layer adjacent to the membranes, as the outflow concentrations at open circuit conditions are not significantly different from those at the inflow. At higher flow velocities, mixing of the boundary layers is improved and the measured OCV approaches the theoretical value. This in contrast to the mixing at very low flow rates (i.e. very low Reynolds numbers).

The stack with spacers has a slightly higher OCV compared to the stack with profiled membranes, although not as significant at all Reynolds numbers. Based on the permselectivity of the individual membranes (Table 1), the OCV could be expected to be the same for both stacks. The small differences are probably due to the better mixing in the stack with spacers. The same is observed for the resistance, as will be discussed later. Poor mixing introduces the same effects (osmosis and co-ion transport) as low Reynolds numbers do.

4.4. Resistance

Fig. 7 shows the area resistances for the stack with profiled membranes and the stack with spacers, divided in R_{ohmic}, $R_{\Delta C}$ and R_{BL}, as function of the Reynolds number.

Fig. 7 shows that R_{ohmic} increases, while $R_{\Delta C}$ and R_{BL} decrease with increasing Reynolds number for both stacks. The decrease of R_{BL} was observed before [5], and is a direct effect of the higher mixing rate at high flow velocities (and thus at high Reynolds numbers). $R_{\Delta C}$ is significant at low Reynolds numbers (even dominant at the lowest Reynolds number), whereas $R_{\Delta C}$ has the smallest contribution at the highest Reynolds number. The decrease of $R_{\Delta C}$ at higher Reynolds numbers is a consequence of the faster re-supply of feed water and can be derived from Eq. (5). Compared to the stack with spacers, the stack with profiled membranes has a significantly lower ohmic resistance, but a distinctively higher boundary layer resistance.

The lower ohmic resistance in case of the profiled membranes was expected, as the profiles provide an ion conductive path, i.e. the spacer shadow effect is eliminated. The ohmic resistance was reduced by approximately 30% compared to the stack with spacers. Although this is a major improvement, the ohmic resistance was even more dramatically reduced when ion conductive spacers were used [6]. This can be due to the relatively high area resistance of the heterogeneous membranes (Table 1; 2.7–5.8 $\Omega\,cm^2$) as used in this experiment, while the experiment with ion conductive spacers in previous research used homogeneous membranes with an area resistance of only 2–3 $\Omega\,cm^2$ [6]. It is expected that profiled membranes with a lower area resistance (for example homogeneous membranes) would result in a more distinct difference when compared to non-conductive spacers is expected.

The boundary layer resistance in the stack with profiled membranes is significantly higher than that in the stack with spacers. This obviously reveals the much better promotion of mixing in the case of the spacers compared to that in the stack with profiled membranes. The spacer filaments act as an obstacle forcing the flow to follow a tortuous path and thus generating additional mixing in the boundary layer. This process is absent when membranes with the current profile are used, leading to an increased R_{BL}.

Overall, the area resistance of the stack with profiled membranes is slightly higher at low Reynolds numbers and slightly lower at high Reynolds numbers than that of the stack with spacers.

4.5. Hydraulic losses

The flow channels as provided by the profiled membranes differ from a hydrodynamic point of view from those provided by the spacers. Spacers are known to cause a large pressure drop over the inflow and outflow of the feed water, indicating large hydraulic friction. The flow along the straight ridges of the profiled membranes is

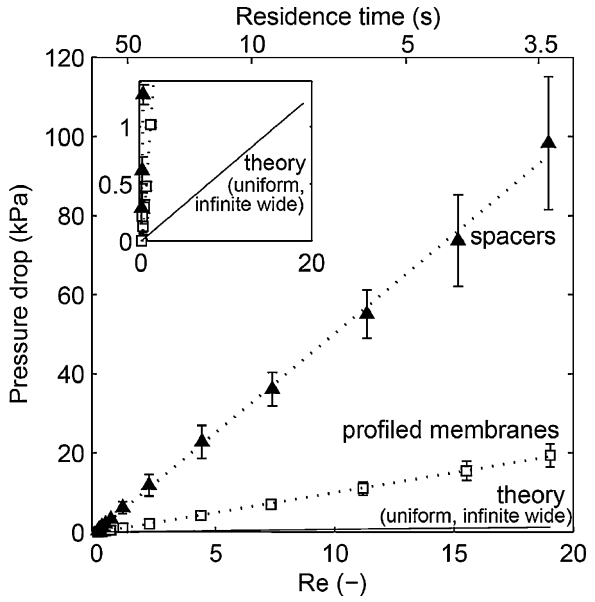

Fig. 8. Pressure drop as a function of the Reynolds number, for a stack with profiled membranes, a stack with spacers and the theoretical pressure drop assuming uniform flow in an infinite wide channel (Eq. (7)). The small axis at the left top shows a zoom for small pressure drops (0–1.5 kPa).

expected to feature less hydraulic friction. Fig. 8 shows the pressure drop over the inflow and outflow of the feed water.

The pressure drop is approximately 4 times lower for the stack with profiled membranes, i.e. the profiled membranes induce significantly less hydraulic friction than the spacers. Still, the pressure drop in the stack with profiled membranes is almost twenty times the theoretical value as calculated for uniform laminar flow as described by Eq. (7). A minor part of this excess can be explained by the finite width of the profiled channels. If the actual geometries of the profiled membranes are considered, instead of an infinite wide channel, the theoretical pressure drop is still approximately 13 times lower than the measured values for the profiled membranes. The latter excess in hydraulic friction is caused at the inflow and outflow of each compartment, where the flow is subject to sharp corners and narrow channels, and thus cannot be considered uniform.

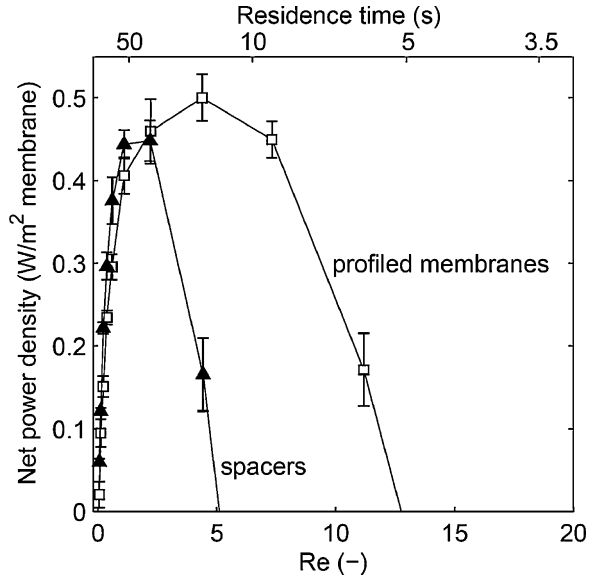

Fig. 9. Net power density as a function of the Reynolds number, for a stack with profiled membranes and a stack with spacers.

The power spent on pumping the feed waters increases with the square of the flow rate (Eqs. (6) and (7)). Subtraction of the power losses for pumping from the gross power density gives the net power density (Fig. 9).

The maximum net power density is approximately 10% higher for the stack with profiled membranes (in the current design) than for the stack with spacers. More important however, is the observation that the peak in net power density shifts towards higher Reynolds numbers for the stack with profiled membranes compared to the stack with spacers, due to the lower hydraulic friction. If the gross power density at this flow rate would increase due to future developments, and thus the efficiency approaches its maximum value (50% for the stacks in this setup), higher flow rates (so higher Reynolds numbers) are inevitable to further improve the power density. The four times lower hydraulic friction for the profiled membranes allows a wider range in Reynolds number. Therefore the profiled membranes have a much better perspective for further improvement in (net) power density.

The relatively low hydraulic friction also allows new flow geometries that improve the gross power density. For example, a smaller inter-membrane distance, i.e. thinner profiled ridges, will significantly enhance the gross power density [5]. Furthermore, new geometries can be designed that induce better mixing than the traditional spacers. Profiling membranes offers a higher degree of freedom to create new profile geometries where a hydrodynamic flow can be combined with efficient mixing in the boundary layers.

5. Conclusions

In this work we show the performance of a reverse electrodialysis (RED) stack using profiled membranes instead of traditionally used non-conductive spacers in between the ion exchange membranes. Hot pressing of commercially available membranes is used to create profiled membranes, which resulted in a slight reduction in permselectivity and significant decrease in resistance. The stack with profiled membranes shows a 30% lower ohmic resistance compared to that with spacers, but the boundary layer resistance is significantly higher. The maximum gross power density of the stack with profiled membranes is slightly higher than that in the stack with spacers. In combination with a lower hydraulic friction, this resulted in a net power density that is 10% higher for the stack with profiled membranes. Even more important is the scope for future development of profiled membranes. The low hydraulic friction enables higher Reynolds numbers than in a stack with spacers. Furthermore, profiling membranes offers a high degree of freedom to create new profile geometries where a hydrodynamic flow can be combined with efficient mixing in the boundary layers.

Acknowledgements

This research is performed at Wetsus, Technological Top Institute for Water technology. Wetsus is funded by the Dutch Ministry of Economic Affairs, the European Union Regional Development Fund, the Province of Fryslân, the City of Leeuwarden and the EZ/Kompas Program of the 'Samenwerkingsverband Noord-Nederland'. The authors are thankful for the support of Alliander, Eneco, Frisia Zout, Fujifilm, Landustrie and Magneto Special Anodes. In addition, the authors thank Dovile Vegelyte for her experimental assistance and thank Joost Veerman, Kristan Goeting, Piotr Długołęcki and Enver Güler for the fruitful discussions.

References

[1] R.E. Pattle, Production of electric power by mixing fresh and salt water in the hydroelectric pile, Nature 174 (1954) 660.
[2] J.W. Post, H.V.M. Hamelers, C.J.N. Buisman, Energy recovery from controlled mixing salt and fresh water with a reverse electrodialysis system, Environmental Science and Technology 42 (2008) 5785–5790.
[3] J. Veerman, M. Saakes, S.J. Metz, G.J. Harmsen, Reverse electrodialysis: performance of a stack with 50 cells on the mixing of sea and river water, Journal of Membrane Science 327 (2009) 136–144.
[4] J.W. Post, C.H. Goeting, J. Valk, S. Goinga, J. Veerman, P.J.F.M. Hack, Towards implementation of reverse electrodialysis for power generation from salinity gradients, Desalination and Water Treatment 16 (2010) 182–193.
[5] D.A. Vermaas, M. Saakes, K. Nijmeijer, Double power densities from salinity gradients at reduced intermembrane distance, Environmental Science and Technology 45 (2011) 7089–7095.
[6] P.E. Długołęcki, J. Dąbrowska, K. Nijmeijer, M. Wessling, Ion conductive spacers for increased power generation in reverse electrodialysis, Journal of Membrane Science 347 (2010) 101–107.
[7] J. Veerman, J.W. Post, M. Saakes, S.J. Metz, G.J. Harmsen, Reducing power losses caused by ionic shortcut currents in reverse electrodialysis stacks by a validated model, Journal of Membrane Science 310 (2008) 418–430.
[8] J. Veerman, M. Saakes, S.J. Metz, G.J. Harmsen, Reverse electrodialysis: a validated process model for design and optimization, Chemical Engineering Journal 166 (2011) 256–268.
[9] J.S. Vrouwenvelder, D.A.G.V.D. Schulenburg, J.C. Kruithof, M.L. Johns, M.C.M.V. Loosdrecht, Biofouling of spiral-wound nanofiltration and reverse osmosis membranes: a feed spacer problem, Water Research 43 (2009) 583–594.
[10] J.W. Post, Blue energy: electricity production from salinity gradients by reverse electrodialysis, in: Environmental Science, Wageningen University, 2009, 222 pp.
[11] O. Kedem, Reduction of polarization in electrodialysis by ion-conducting spacers, Desalination 16 (1975) 105–118.
[12] V.V. Nikonenko, N.D. Pismenskaya, A.G. Istoshin, V.I. Zabolotsky, A.A. Shudrenko, Description of mass transfer characteristics of ED and EDI apparatuses by using the similarity theory and compartmentation method, Chemical Engineering and Processing 47 (2008) 1118–1127.
[13] C. Larchet, V.I. Zabolotsky, N. Pismenskaya, V.V. Nikonenko, A. Tskhay, K. Tastanov, G. Pourcelly, Comparison of different ED stack conceptions when applied for drinking water production from brackish waters, Desalination 222 (2008) 489–496.
[14] H. Strathmann, Electrodialysis, a mature technology with a multitude of new applications, Desalination 264 (2010) 268–288.
[15] P.E. Długołęcki, K. Nijmeijer, S.J. Metz, M. Wessling, Current status of ion exchange membranes for power generation from salinity gradients, Journal of Membrane Science 319 (2008) 214–222.
[16] P. Sistat, G. Pourcelly, Chronopotentiometric response of an ion-exchange membrane in the underlimiting current-range. Transport phenomena within the diffusion layers, Journal of Membrane Science 123 (1997) 121–131.
[17] J. Veerman, M. Saakes, S.J. Metz, G.J. Harmsen, Electrical power from sea and river water by reverse electrodialysis: a first step from the laboratory to a real power plant, Environmental Science and Technology 44 (2010) 9207–9212.
[18] V.I. Zabolotsky, S.A. Loza, M.V. Sharafan, Physicochemical properties of profiled heterogeneous ion-exchange membranes, Russian Journal of Electrochemistry 41 (2005) 1053–1060.
[19] J.N. Weinstein, F.B. Leitz, Electric power from differences in salinity: the dialytic battery, Science 191 (1976) 557–559.
[20] P.E. Długołęcki, A. Gambier, K. Nijmeijer, M. Wessling, Practical potential of reverse electrodialysis as process for sustainable energy generation, Environmental Science and Technology 43 (2009) 6888–6894.
[21] J. Veerman, R.M.D. Jong, M. Saakes, S.J. Metz, G.J. Harmsen, Reverse electrodialysis: comparison of six commercial membrane pairs on the thermodynamic efficiency and power density, Journal of Membrane Science 343 (2009) 7–15.
[22] J. Balster, M.H. Yildirim, D.F. Stamatialis, R. Ibanez, R.G.H. Lammertink, V. Jordan, M. Wessling, Morphology and microtopology of cation-exchange polymers and the origin of the overlimiting current, Journal of Physical Chemistry B 111 (2007) 2152–2165.
[23] J. Balster, D.F. Stamatialis, M. Wessling, Membrane with integrated spacer, Journal of Membrane Science 360 (2010) 185–189.